Proceedings of the ASME 2020 International Mechanical Engineering Congress and Exposition IMECE2020 November 16-19, 2020, Portland, OR, USA

IMECE2020-23520

SEPARATION OF NON-VIABLE CHINESE HAMSTER OVARY (CHO) CELLS USING DIELECTROPHORESIS IN A DETERMINISTIC LATERAL DISPLACEMENT RATCHET

Mohammed Khan¹, Xiaolin Chen¹, School of Engineering and Computer Science, Washington state University Vancouver, WA. United States

ABSTRACT

Chinese hamster ovary (CHO) cell is the most widely used mammalian cell line for commercial production of therapeutic protein. Any presence of non-viable cells in culture medium may adversely affect subsequent functionality of these proteins. Therefore, separation of non-viable cells from suspending medium is critical in biopharmaceutical and biomedical sectors. One such method termed Deterministic Lateral Displacement has already shown promising capabilities in separating cells based on the cell size difference by taking advantage of the predictable flow laminae. However, in cases where size overlaps between viable and non-viable cells are present, separation based solely on size suffers and high-resolution separation techniques are required. Dielectrophoresis, one of the most widely used nonlinear electro-kinetic mechanism, has the potential to manipulate the same size cells depending on the dielectric properties of individual cells. In this work, we demonstrated that a DLD device can be combined with a frequency-based AC electric field to perform high resolution continuous separation of non-viable CHO cells from the viable or productive cells. The behavior of the coupled DLD-DEP device is further investigated by employing numerical simulation to check the effect of geometrical parameters of the DLD arrays, velocities of the flow field and required applied voltages. A moderate row shift fraction with velocity 700µm/s provided a good separation behavior without any trapping. The cell viability was also ensured by maintaining proper electric field which otherwise may cause cell loss due to ion leakage. Our developed numerical model and presented results lay the groundwork for design and fabrication of high resolution DLD-DEP microchips for enhanced separation of viable and nonviable cells.

Jie Xu²

Department of Mechanical and Industrial Engineering, University of Illinois at Chicago, Chicago, United States

Keywords: CHO cell, Dielectrophoresis, Deterministic Lateral Displacement.

1. INTRODUCTION

Therapeutic protein has widespread use in the diagnostics and treatment for various human diseases and has become a vital part of biopharmaceuticals industry. Although a variety of other alternative mammalian cell lines exist, such as mouse myelomaderived NS0, baby hamster kidney, and transgenic animal, CHO cells have been the primary hosts for the commercial production of therapeutic proteins for decades. According to Javapal et al. in 2007, nearly 70% of all recombinant therapeutic proteins produced were made in Chinese hamster ovary (CHO) cells [1]. But due to apoptosis or programmed cell death, many CHO cell lines undergo morphological alterations and lose viability. The presence of non-viable CHO cells after cell cultivation in the cultural medium impair subsequent results/functionality of stem cell grafts [2]. So, cell retention or separation techniques should be incorporated with the continuous animal cell culture processes.

In recent years, the emergence of the field of microfluidics has extended its application to the label-free methods of cell separation studies. One promising passive particle separation technique is Deterministic lateral displacement (DLD). Deterministic lateral displacement is a technology that employs different geometry of post array for lateral migration of cells based on size within a microchannel to facilitate separation of particles larger and smaller than a designed critical diameter [3]. This technique was pioneered by Huang et al. in 2004 and since then it has been extensively studied [4]. Many research groups have explored this technique to apply it for different purposes including biological cell separation i.e., circulating tumor cells [16], white blood cells (WBCs), red blood cells (RBCs),

¹ Contact author: mohammed.khan2@wsu.edu

parasites, platelets, bacteria and exosomes. Both biological and non-biological particles were successfully separated in case of DLD devices. But this device suffers when cells of similar sizes need to be separated. Besides, the unpredictability of the device performance at high throughput due to flow-induced cell deformation is also a concern [5].

Thus, a shift from passive DLD to active DLD was imminent to achieve more efficiency. In recent years, while many label-free approaches suffer from overlaps in physical properties of cells, dielectrophoresis (DEP) showed excellent results by exploiting the dielectric differences of viable and non-viable cells in isolating them from each other [6]. Due to apoptosis triggered by nutrient depletion during/after batch culture of cells, apoptotic CHO cells have a significant change in their dielectric spectrum compared to viable CHO cells [7,8]. Taking leverage from these findings, Cemezar et al. in 2010 showed one such Dielectrophoretic microchamber that was capable of separating non-viable cells with 93% efficiency [9]. However, this microchamber used electrode-based dielectrophoresis or e-DEP where possibility of fouling and bubble formation exists [10]. Chamber volume constraints also hindered the continuous separation mode forcing to stick only to batch mode of operation. On the other hand, insulator-based Dielectrophoresis or i-DEP can facilitate differential guidance to both viable and non-viable cells into two different directions resulting in higher throughput/continuous separation. The use of remote electrode also eradicates the possibility of any fouling of electrodes in the zone of interest, as seen in e-DEP devices [11].

Thus, in this study, an investigation of the applicability of iDEP with classical DLD like array of insulating post was performed for separation of viable and non-viable CHO cells. Although there have been prior attempts to couple these two phenomena, none of them address the suitability with CHO cells. To name some, Cummings et al. showed for the first time the use of DEP with insulating post and discussed that particle streaming and trapping could be manipulated by a balance between electrokinetic flow and dieletrophoresis. DC electric field was utilized for demonstration in their case [12]. Following this work, Beech et al. demonstrated a tunable device to decrease the critical size of DLD with the use of AC electric field [11]. Recently, Calero et al. described a frequency-dependent tunable AC electrokinetic biased DLD device. They observed a separation due to electrophoretic (EP)/electroosmotic (EO) forces at low frequency and dielectrophoresis dominated separation at a high frequency of the AC electric field [13]. None of the work addresses the issue with biological cells, especially mammalian cells. In very recent studies, Aghamooo et al. analyzed the performance of a frequency-controlled alternative voltage (AC) iDEP design by changing micro-posts geometry, electrode setups, and flow field characteristics to demonstrate a separation between MDA-231 breast cancer cells and WBCs [10,14]. Such a frequency-dependent phenomenon can be exploited to construct a device with adequate separation efficiency and good resolution for long term stable operation in the bio-reactor for mammalian CHO cells.

In this work, a numerical modeling is performed initially by utilizing a three-shell dielectric model for the CHO cell. Based on dielectric spectrum, a crossover frequency and appropriate medium conductivity are identified for viable cells. Next, best design criteria for effective separation of both of this cell population has been analyzed, keeping in mind of the viability of separated cells. Then, a DLD-DEP device was proposed for continuous separation of viable CHO cells from the non-viable population based on crossover frequency of viable cells.

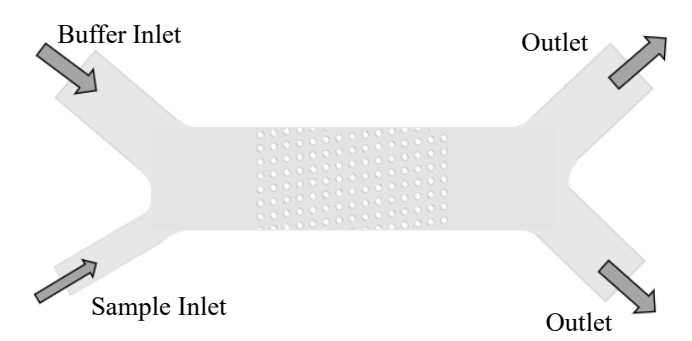


Figure 1: Model Description and geometry definition of the DLD-DEP micro-device.

2. THEORY

The mechanism of separation by DLD is pretty straightforward. In the design, it consists of several pillar-shaped micro-posts where each post is displaced laterally from the predecessor by a distance called $\Delta\lambda$ as shown in Fig. 1. As the flow moves through the channel it becomes bifurcated. Separate flow lanes equal to the number periodicity, N of the geometry are created between the post where each flow lamina defined by streamline carries the same fluid flux. Assumption of the parabolic flow profile between the post and the width of the first flow lane can deterministically indicate particle migration mode. As particles enter into the post-gaps and interact with the pillars, the particle with a radius smaller than the first width of the streamline remains in the initial streamline and follows the zigzag mode. On the other hand, particle with radius larger than the first streamline width tend to shift laterally to the next flow lane called the displacement or bumped mode. Mimicking the same action in several consecutive posts the larger particle can be displaced further. The transition at which particle switch to bump mode is known as Critical diameter of the particle. Davis et al. derived an empirical formula for the critical diameter of DLD which is equivalent to the first streamline width based on the geometrical parameters of the array, assuming an array of circular posts as [3]

$$D_c = 1.4G \,\varepsilon^{0.48} \tag{1}$$

where, $\varepsilon = \Delta \lambda / \lambda$ defines the lateral row shift, $\lambda = D_p + G$ being the center to center distance between posts, G is the gap between posts and D_p is the post diameter.

Dielectrophoresis is the movement of polarizable cells in a non-uniform electric field. For conventional DEP the time average DEP force acting on a spherical cell in a nonhomogeneous electrical field, E can be expressed by the following equation:

$$\langle F_{DEP}(t) \rangle = 2\pi \varepsilon_{med} r^3 Re[K_{CM}(\omega)] \nabla |E|^2$$
 (2)

where, ε_{med} and r are permittivity of the suspending medium and radius of spherical cell, respectively. $Re(K_{CM})$ refers to the real part of the Clausius-Mossotti factor defined as:

$$K_{CM}(\omega) = \frac{\overline{\varepsilon}_{cell} - \overline{\varepsilon}_{med}}{\overline{\varepsilon}_{cell} + 2\overline{\varepsilon}_{med}}$$
(3)

In which, $\bar{\epsilon}_{cell} = \epsilon_{cell} - j \frac{\sigma_{cell}}{\omega}$, $\bar{\epsilon}_{med} = \epsilon_{med} - j \frac{\sigma_{med}}{\omega}$ denotes the frequency dependent complex permittivity of the cell and the medium respectively and ω is the angular frequency. If the cell is more polarizable than the medium, a positive DEP force will exert on the cell that will attract it to the high electric field regions. On the other hand, if the medium is more polarizable than the cell, a negative DEP force will be applied to the cell and they will be pushed away from high electric field regions. Besides, the real part of Clausius-Mossotti factor can be equal to zero for a definite value of applied frequency called crossover frequency which results in zero DEP force applied to the cell.

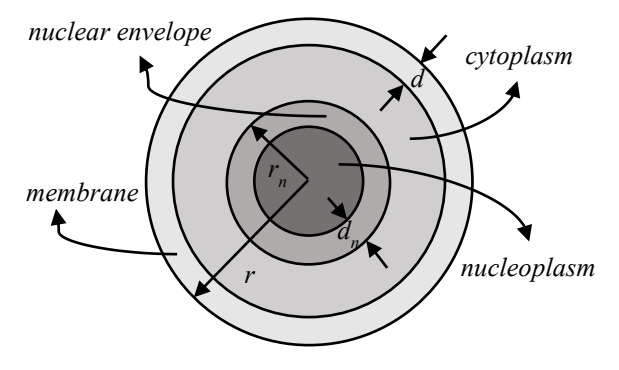


Figure 2: Multi-shell model of CHO cell consisting of nucleoplasm, nuclear envelope, cytoplasm and membrane.

Biological cells however, composed of different parts such as cell nucleus, nuclear envelope, cytoplasm, and thin membrane shown in Fig. 2. Each part has different dielectric properties. So, to characterize biological cells precisely to calculate complex permittivity of cell, $\bar{\epsilon}_{cell}$ a multi-shell model is used [15]. According to the model, the complex permittivity of the cell can be expressed as

$$\overline{\varepsilon}_{cell} = \overline{\varepsilon}_m \frac{\left(\frac{r}{r-d}\right)^3 + 2\left(\frac{\overline{\varepsilon}_{i-ne} - \overline{\varepsilon}_m}{\overline{\varepsilon}_{i-ne} + \overline{\varepsilon}_m}\right)}{\left(\frac{r}{r-d}\right)^3 - \left(\frac{\overline{\varepsilon}_{i-ne} - \overline{\varepsilon}_m}{\overline{\varepsilon}_{i-ne} + \overline{\varepsilon}_m}\right)}$$
(4)

$$\overline{\varepsilon}_{i-ne} = \overline{\varepsilon}_{i} \frac{\left(\frac{r-d}{r_{n}}\right)^{3} + 2\left(\frac{\overline{\varepsilon}_{ne-n} - \overline{\varepsilon}_{i}}{\overline{\varepsilon}_{ne-n} + \overline{\varepsilon}_{i}}\right)}{\left(\frac{r-d}{r_{n}}\right)^{3} - \left(\frac{\overline{\varepsilon}_{ne-n} - \overline{\varepsilon}_{i}}{\overline{\varepsilon}_{ne-n} + \overline{\varepsilon}_{i}}\right)}$$

$$\overline{\varepsilon}_{ne-n} = \overline{\varepsilon}_{ne} \frac{\left(\frac{r_{n}}{r_{n} - d_{n}}\right)^{3} + 2\left(\frac{\overline{\varepsilon}_{n} - \overline{\varepsilon}_{ne}}{\overline{\varepsilon}_{n} + \overline{\varepsilon}_{ne}}\right)}{\left(\frac{r_{n}}{r_{n} - d_{n}}\right)^{3} - \left(\frac{\overline{\varepsilon}_{n} - \overline{\varepsilon}_{ne}}{\overline{\varepsilon}_{n} + \overline{\varepsilon}_{ne}}\right)}$$
(6)

$$\bar{\varepsilon}_{ne-n} = \bar{\varepsilon}_{ne} \frac{\left(\frac{r_n}{r_n - d_n}\right)^3 + 2\left(\frac{\bar{\varepsilon}_n - \bar{\varepsilon}_{ne}}{\bar{\varepsilon}_n + \bar{\varepsilon}_{ne}}\right)}{\left(\frac{r_n}{r_n - d_n}\right)^3 - \left(\frac{\bar{\varepsilon}_n - \bar{\varepsilon}_{ne}}{\bar{\varepsilon}_n + \bar{\varepsilon}_{ne}}\right)}$$
(6)

r is the cell radius, r_n is the nuclear radius, d is the membrane thickness and d_n is the nuclear envelope thickness, $\bar{\epsilon}_{i-ne}$ is the equivalent complex permittivity of cytoplasm and nuclear envelope, $\bar{\epsilon}_m$ is the complex permittivity of the membrane, $\overline{\varepsilon}_{ne-n}$ is the equivalent complex permittivity of nucleoplasm and nuclear envelope, $\bar{\epsilon}_n$ is the complex permittivity of the nucleoplasm, $\bar{\varepsilon}_i$ is the complex permittivity of the cytoplasm and $\overline{\varepsilon}_{ne}$ is the complex permittivity of the nuclear envelope.

3. NUMERICAL MODEL DESCRIPTION

To thoroughly investigate the applicability of DEP with classical DLD and its feasibility for continuous separation of viable and non-viable CHO cells, a 2D micro-geometry is designed and modeled using commercial computer software package COMSOL Multiphysics 5.3 (COMSOL Inc. Burlington, MA). As shown in Fig. 1., two inlets are used for the 2D microgeometry - one for introduction of the buffer and another for the sample. Arrays of micro-pillars are placed in the direction of the fluid flow. A horizontal voltage is applied to generate an electric field in the same direction as the fluid flows. For this study, the gap size between the posts and post diameter is fixed at 40 µm; while the row shift fraction (ε) along with applied voltage and buffer velocity are kept variable for design analysis. Finally, two outlets are placed at the end of the arrays to collect the two different population of cells.

Both Fluid Flow and AC/DC modules is used initially to solve for the fluid-flow fields and electric fields in the domain. The velocity field is solved by using the Navier-Stokes along with continuity equations without the gravity and buoyancy effect as following:

$$\rho \left[\frac{\partial \mathbf{v}}{\partial t} + \mathbf{v} \cdot \nabla \mathbf{v} \right] = -\nabla p + \eta \nabla^2 \mathbf{v}$$

$$\nabla \cdot \mathbf{v} = 0,$$
(8)

where, ρ , ν , p and η are the fluid density, velocity, pressure, and viscosity, respectively. This Navier-Stokes equation has further simplified to its creeping flow regime where the inertial effects are negligible and a steady state case is considered.

On the other hand, the electric field, E is obtained by solving the following set of equations:

$$\mathbf{E} = -\nabla \phi \tag{9}$$

$$\nabla \cdot (\varepsilon_m \mathbf{E}) = \rho_E \tag{10}$$

$$\nabla \cdot (\varepsilon_m \mathbf{E}) = \rho_E \tag{10}$$

$$\frac{\partial \rho_E}{\partial t} + \nabla \cdot (\sigma \mathbf{E}) = 0 \tag{11}$$

where, ϕ is the electric potential, ε_m is the medium permittivity, ρ_E is the net volumetric free charge density, and σ is the medium conductivity.

Next, the trajectories of individual cells exposed to the combined force-field of the Drag and DEP were simulated by numerical modeling. Previously solved flow and electric field solutions are utilized for this purpose. The motion of a cell in an incompressible, viscous liquid subjected to a nonuniform electric field can be expressed by utilizing Newton's second law as

$$m_{cell} \frac{d}{dt}(v_{cell}) = F_{Drag} + F_{DEP}$$
 (12)

where, the drag force experienced by the spherical cells can be calculated using stokes drag law:

$$F_{Drag} = 6\eta r \pi (v - v_{cell}) \tag{13}$$

 η being the fluid viscosity, r is the cell radius, v and v_{cell} are the velocities of the fluid and the cell, respectively.

Before studying the separation of viable and non-viable CHO cells, the dielectric spectrum of both the cells need to be analyzed using the multi-shell modeling. For that, the mechanical and electrical properties of these cell are specified

Table 1. Parameters of viable and non-viable CHO cell for modeling of dielectric spectrum [7, 9]

below:

Parameter	Viable	Non-viable
<i>r</i> (µm)	6.5	5.53
$r_n (\mu m)$	3.53	
$d_n(\mu m)$	40	
d (µm)	5	4.25
$\sigma_{m} (\mu S/m)$	3	15
$\sigma_{i}\left(S/m\right)$	0.32	0.17
σ_{ne} (mS/m)	6	30
$\sigma_n(S/m)$	1.35	0.17
ε_m (F/m)	$6.80\varepsilon_0$	
ε_i (F/m)	$60\epsilon_0$	
ε_{ne} (F/m)	$28\epsilon_0$	
$\varepsilon_n(F/m)$	$52\varepsilon_0$	

4. RESULTS AND DISCUSSION

To analyze and perform a comprehensive study of the DLD-DEP device, different aspects of the design have been explored. The combined effect of both DLD and DEP will influence the cell trajectory. Frequency and electric field are the two key factors to consider for the current DEP configuration, which is based on AC-iDEP design. On the other hand, for the DLD device buffer velocity, device's row shift fraction will play a critical role in changing cell paths in the fluid field. The effect of

these factors will be analyzed in subsequent sections to provide design consideration for the separation of viable and non-viable CHO cells.

4.1 Frequency Effect

To select appropriate frequency for the micro-device, first of all the DEP response is checked for both CHO cells utilizing the multi-shell model as discussed previously. The DEP response is the plot of real part of Clausius-Mossotti (CM) factor that denotes whether a cell will have pDEP, nDEP or zero DEP by Eq. 2. The parameters required for the modeling are collected from previous study [7, 9] and specified in Table.1. Among them medium conductivity has substantial effect on the spectrum of DEP as seen from the plot of real part of Clausius-Mossotti factor in Fig. 3. for both viable and non-viable cells. Besides, the spectrum of both type of cells shows significant difference with applied electric frequency. For separation purpose both population of cells need to experience opposite DEP forces which will attract one cell population and repel other population. It will result in trapping of one cell population causing a decrease

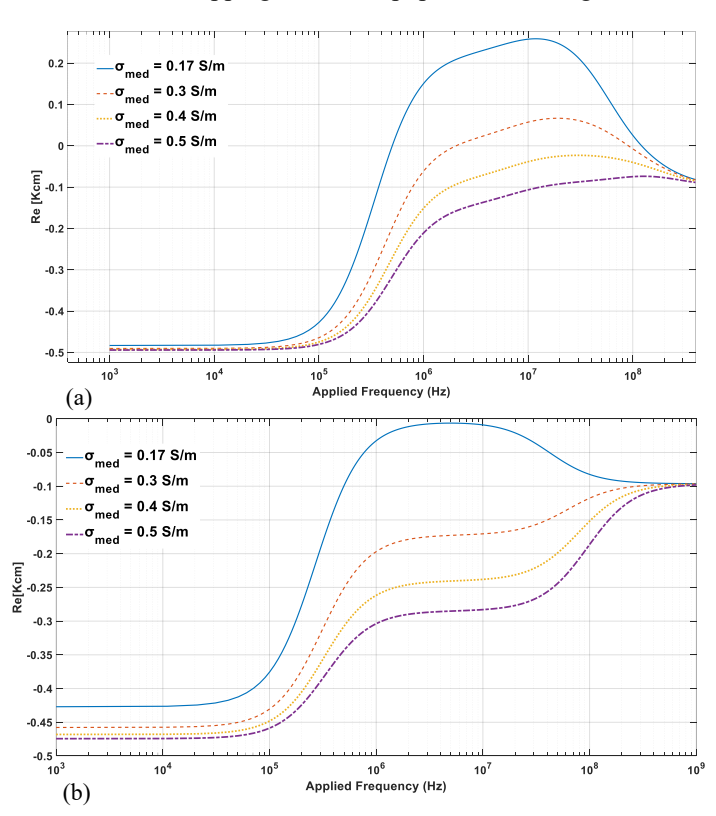


FIGURE 3: Variation of the real part of Clausius-Mossotti factor with different medium conductivity of 0.17 S/m, 0.3 S/m, 0.4 S/m and 0.5 S/m for a) viable CHO cell, b) non-viable CHO cell using multi-shell model.

in the throughput. Another case would be to apply zero DEP force to one cell and negative DEP on the other. It can cause continuous separation of both cell populations as no trapping will occur due to pDEP. The trapping due to nDEP can be avoided with drag force adjustments which will be discussed later. As this

study is focusing on continuous separation of viable and non-viable CHO cells, careful selection of medium conductivity and applied frequency is important so-that one cell has the zero DEP force and another one has the negative DEP force.

From Fig. 3. it can be seen that irrespective of medium conductivity and field frequency, non-viable cells will always experience nDEP. Same phenomenon goes with the viable cell with medium conductivity of 0.4 S/m and 0.5 S/m. Choosing a medium conductivity between this two for viable cell will cause both population of cell to have the nDEP force. This will result no separation based on dielectric properties. In cases of medium conductivity 0.17 S/m and 0.3 S/m, viable CHO cells showed a wide range of CM spectrum ranging from negative DEP to positive DEP, including the zero DEP. However, for 0.3 S/m medium conductivity, a zero DEP force can be achieved at a relatively high field frequency known as crossover frequency. Setting a high frequency in a micro-device may have adverse effect on the viability of the cell by introducing thermal gradient

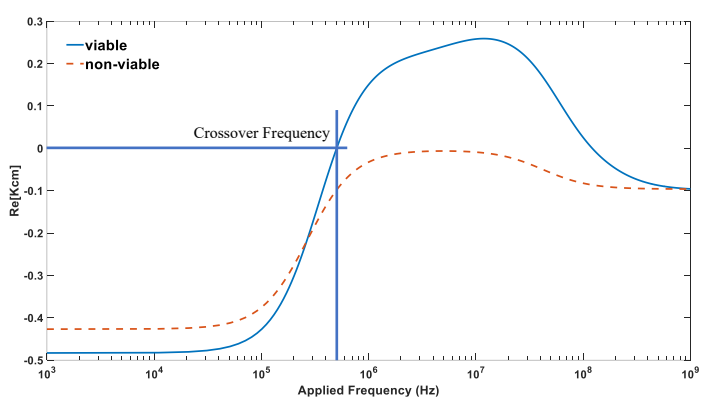


Figure 4: Real part of Clausius-Mossotti factor against applied field frequency at medium conductivity 0.17 S/m for both viable and non-viable CHO cell using multi-shell modelling. Parameters listed in Table. 1. Equation utilized from Eqn. 3-6.

in the domain [14]. So, to achieve continuous operation and maintain cell viability in our device, the best choice would be to select medium electrical conductivity as 0.17 S/m.

In Fig. 4. the CM factor for both viable and non-viable cell have been plotted against field frequency at medium electric conductivity of 0.17 S/m. It is evident that at the crossover frequency (= 5×10^5 Hz) of the viable cell, an nDEP force will act on the non-viable cell and a zero DEP on the viable one. This nDEP will repel the non-viable cell from high electric field region during each interaction with the micro-post causing them to change their trajectory. On the other hand, due to zero DEP force, viable cells will follow the flow field trajectory ultimately causing both populations to separate at the outlet.

4.2 Effect of Row shift fraction, Flow field and Applied voltage/Electric field

In this coupled DLD-DEP device, drag force and DEP force are the primary contributors for the manipulation of the trajectory of the cell. The drag force arises due to the fluid flowing in the micro-device and influenced due to the presence

of micro-pillars. Therefore, the effect of drag on the device can be adjusted by flow field along with row shift fraction. It is to be mentioned here that the row shift fraction can tune the critical size of cell in the device according to Eq. 1. Also, change in the velocity of the buffer changes the flow field distribution causing the drag force experienced by the cells to enhance or to decrease. On the other hand, the DEP influence on the device relies on careful consideration of the applied frequency and AC voltage at inlet and outlet. The effect of applied frequency is discussed earlier. Due to the presence of insulating posts in the geometry, the applied AC voltage generates a nonuniform electric field in the domain. The distribution of the electric field can be seen in Fig. 5. Each post has a high electric field region at top and bottom curvatures and low electric field region at leading and trailing curvatures. The function of the high electric field region is to attract cell with pDEP and repel cell with nDEP and vice versa for low electric field region. Note that the DEP force depends on the gradient of the squared electric field according to Eq. 2. As such, the DEP strength can be regulated by changing the applied AC voltage which contributes to the electric field.

In order to have proper and continuous separation between viable and non-viable cell, careful adjustment is needed between the drag and nDEP force for the coupled device. A trapping regime may occur if the nDEP force is too high compared to the drag force for a cell under consideration. The resulting nDEP can attract the non-viable cell in the low electric field region around the post. This behavior can increase clogging in the device. The trapping regime can be avoided if the aforementioned parameters- row shift fraction, flow field and applied voltage that influence the drag and DEP forces are adjusted in such a way that one population of cell go in the bumped mode and another

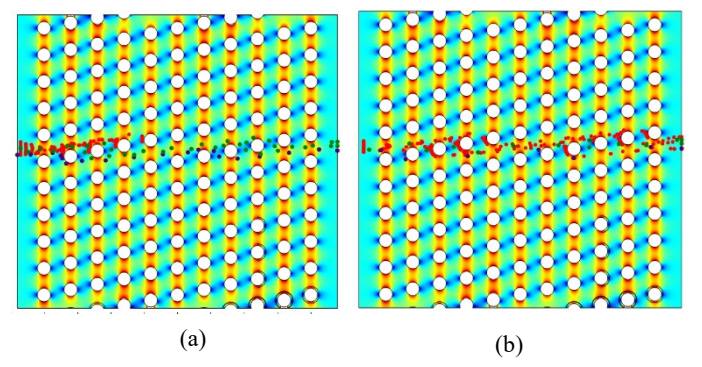


Figure 5: Particle trajectory for both viable and nonviable cell at row shift fraction, $\varepsilon=1/5$, and applied Voltage = 30V; a) Buffer Velocity = $100\mu\text{m/s}$ and b) Velocity = $300\mu\text{m/s}$. Red ones denote the non-viable CHO cells and Green/Purple ones denote the viable cells. Left figure a) is showing how the non-viable cells are trapping around the post for buffer velocity of $100~\mu\text{m/s}$. Right one b) is showing both particles are following the zigzag pattern idicating the dominancy of hydrodynamic forces.

follow the zigzag one. One way of achieving that phenomenon, as discussed earlier, is to set the applied frequency = crossover frequency (= 5×10^5 Hz) of the viable cell. Numerical simulations have been performed to check the system behavior causing by the change in parameters - row shift fraction, flow field and

applied voltage. Note that all cells are below the initial theoretical critical size of the micro-device which means in the absence of electric field all cells will follow the fluid stream path. The electric field is always maintained below 5×10^5 V/m to overcome cell losses due to ion leakage [10]. Our primary focus would be to look for appropriate velocity, applied voltage and row shift fraction range so that it can cause the non-viable cell to migrate into bump mode leaving the viable one to have the zigzag mode.

4.2.1 Selection of Row shift fraction

For a case with high row shift fraction, $\varepsilon = 1/5$, no continuous separation is observed with any electric field and velocity combination. Two different scenarios are illustrated in Fig. 5. In one case a low buffer velocity i.e., 100µm/s is introduced in the micro-device and another case being a velocity of 300µm/s. Results with the external applied voltage maintained at 30V are shown only. Other voltages exhibited the same behavior. For the case where the velocity is 100 µm/s, all the nonviable CHO cells (Red one) tend to be trapped around the post near leading edge. This edge zone is characterized by the low electric field region. As discussed earlier, low electric field region attracts cell with nDEP and repels cell with pDEP. In this device, non-viable cells are experiencing nDEP force which at this row shift fraction, $\varepsilon = 1/5$ and buffer velocity = $100\mu m/s$ is too strong against the drag force. The low electric field region distribution is also quite high for row shift fraction, $\varepsilon = 1/5$ compared to other cases - another reason behind trapping. If the buffer velocity is increased same behavior exists till 300 µm/s. At 300µm/s, both viable and non-viable cells will have the zigzag mode. The nDEP force could not overcome the hydrodynamic effects to drift the non-viable cell into the bumped mode. The stronger drag force conveys both population of cells through the zigzag mode ultimately resulting no separation. So, for this row shift fraction continuous separation is not feasible.

Now, if row shift fraction is decreased to lower value, the corresponding critical size of the DLD will fall below the size of the CHO cells. This will result in bumped mode for both population of cells irrespective of the dielectric properties. Thus, low row shift fraction is also not desirable as it will be counterproductive for our design consideration. Consequently, a higher row shift fraction but lower than $\epsilon=1/5$ is chosen. Row shift fraction in a range of $\epsilon=1/8\sim 1/10$ show good separation behavior in the next section.

4.2.2 Selection of Flow field and Applied voltage

Figure 6. shows the maximum acceptable velocity and corresponding applied voltage for continuous migration of non-viable cell into the next fluid lamina for row shift fraction, $\epsilon = 1/8$ and 1/10. It is evident that for each externally applied voltage, there is a maximum velocity beyond which non-viable cells cannot have the bumped mode —a minimum velocity below which cells get trapped near the post. As discussed earlier, this device controls the trajectory of the individual cell through a competition between drag and the DEP force. At a particular applied voltage when cell switched to zigzag mode from the

bumped one due to increase in velocity, reason behind is that the drag force has dominancy over the DEP force. On the other hand, when cells get trapped, nDEP force becomes dominant and it attracts cells to low electric field region to trap them. These observations clarify that there is a region between these two zones where non-viable cell have the bumped mode. Due to its presence a continuous separation takes place between the viable and non-viable cell population at outlet. Again, with the intensification of the applied voltage which strengthen the gradient of the electric field, the maximum velocity of the buffer can be increased. This will eventually maximize the throughput of the micro-device. Similar explanations also work for row shift fraction, $\varepsilon = 1/10$. However, the higher velocities can be achieved with row shift fraction, $\varepsilon = 1/10$ as seen in Fig. 6(b).

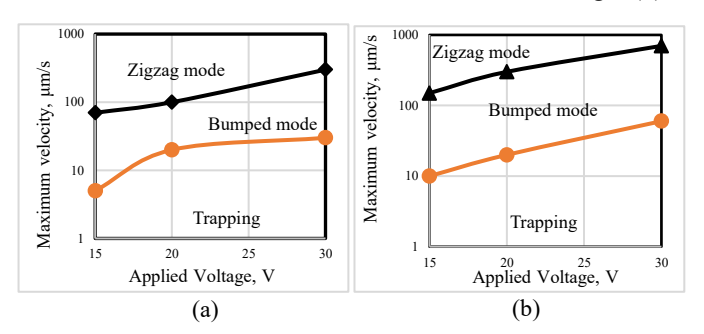


Figure 6: Non-viable cell trajectory indicating curve with different combination of applied voltage and velocity for the DLD-DEP device a) $\varepsilon = 1/8$; b) $\varepsilon = 1/10$

4.3 Separation of Viable and Non-viable CHO cell using DLD-DEP device

Finally, in order to demonstrate the applicability of the proposed DLD-DEP device both viable and non-viable cells are

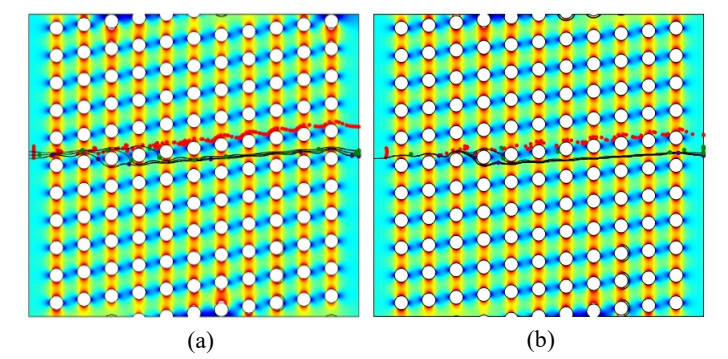


Figure 7: Particle trajectory for both viable and non-viable cell at applied Voltage = 30V; a) Row shift fraction, $\varepsilon = 1/8$, and Buffer Velocity = $300 \mu \text{m/s}$ and b) Row shift fraction, $\varepsilon = 1/10$, and Velocity = $700 \mu \text{m/s}$. Red and purple ones denote the non-viable CHO cells and Green ones denote the viable cells.

introduced in two devices of row shift fraction, $\epsilon = 1/8$ and 1/10 as shown in Fig. 7. A 30V is applied between the inlet and outlet in both devices. The resulting electric field is 76746 V/m which is within the limit for cell retention as mentioned earlier. To show the overlapped-size separation ability, viable cell with the size equal to the non-viable one is also injected in addition to its

original one. A maximum buffer velocity of $300\mu m/s$ and $700\mu m/s$ is achieved in the two devices of row shift fraction, $\epsilon=1/8$ and 1/10 respectively. Higher throughput can be achieved with row shift fraction, $\epsilon=1/10$ while $\epsilon=1/8$ gives wide migration angle at outlet. Both the device shows good separation behavior demonstrating the effectiveness of the coupled DLD-DEP design for the separation of viable and non-viable CHO cells.

5. CONCLUSION

In this study, we developed a DLD-DEP design based on frequency-controlled AC electric field to demonstrate continuous separation of non-viable CHO cell from the viable one. The proposed design takes the advantage of both the DLD and DEP to influence the trajectory of the cells in the buffer fluid domain. The effects of row shift fraction, fluid flow and applied external voltage were analyzed to arrive at the best design criteria for the separation of the CHO cells.

ACKNOWLEDGEMENTS

The authors would like to thank Sarah Rue at the Genomics Institute of the Novartis Research Foundation (GNF) for the interesting discussions on the topic of CHO cells.

REFERENCES

- [1] Jayapal, KP, Wlaschin, KF, Hu, WS & Yap, MGS 2007, 'Recombinant protein therapeutics from CHO Cells 20 years and counting', Chemical Engineering Progress, 103(10), pp. 40-47.
- [2] De Boer, F., Dräger, A., Pinedo, H., Kessler, F., Monnee-van Muijen, M., Weijers, G., Westra, G., van der Wall, E., Netelenbos, T., Oberink, J., Huijgens, P., and Schuurhuis, G., 2002, "Early Apoptosis Largely Accounts for Functional Impairment of CD34+Cells in Frozen-Thawed Stem Cell Grafts", Journal of Hematotherapy & Stem Cell Research, 11(6), pp. 951-963.
- [3] Davis, J., 2008, "Microfluidic Separation of Blood Components Through Deterministic Lateral Displacement", Doctor of Philosophy, Princeton University.
- [4] Huang, L., 2004, "Continuous Particle Separation Through Deterministic Lateral Displacement", Science, 304(5673), pp. 987-990.
- [5] Liu, Z., 2013, "Rapid isolation of cancer cells using microfluidic deterministic lateral displacement structure", Biomicrofluidics, 7(1), p. 011801.
- [6] Tada, S., Hayashi, M., Eguchi, M., and Tsukamoto, A., 2017, "High-throughput separation of cells by dielectrophoresis enhanced with 3D gradient AC electric field", Biomicrofluidics, 11(6), p. 064110.
- [7] Braasch, K., Nikolic-Jaric, M., Cabel, T., Salimi, E., Bridges, G., Thomson, D., and Butler, M., 2013, "The changing dielectric properties of CHO cells can be used to determine early apoptotic events in a bioprocess",

- Biotechnology and Bioengineering, 110(11), pp. 2902-2914.
- [8] Salimi, E., Braasch, K., Fazelkhah, A., Afshar, S., Saboktakin Rizi, B., Mohammad, K., Butler, M., Bridges, G., and Thomson, D., 2018, "Single cell dielectrophoresis study of apoptosis progression induced by controlled starvation", Bioelectrochemistry, 124, pp. 73-79.
- [9] Čemažar, J., Vrtačnik, D., Amon, S., and Kotnik, T., 2011, "Dielectrophoretic Field-Flow Microchamber for Separation of Biological Cells Based on Their Electrical Properties", IEEE Transactions on NanoBioscience, 10(1), pp. 36-43.
- [10] Aghaamoo, M., Aghilinejad, A., Chen, X., and Xu, J., 2019, "On the design of deterministic dielectrophoresis for continuous separation of circulating tumor cells from peripheral blood cells", ELECTROPHORESIS, 40(10), pp. 1486-1493.
- [11] Beech, J., Jönsson, P., and Tegenfeldt, J., 2009, "Tipping the balance of deterministic lateral displacement devices using dielectrophoresis", Lab on a Chip, 9(18), p. 2698.
- [12] Cummings, E., and Singh, A., 2003, "Dielectrophoresis in Microchips Containing Arrays of Insulating Posts: Theoretical and Experimental Results", Analytical Chemistry, 75(18), pp. 4724-4731.
- [13] Calero, V., Garcia-Sanchez, P., Honrado, C., Ramos, A., and Morgan, H., 2019, "AC electrokinetic biased deterministic lateral displacement for tunable particle separation", Lab on a Chip, 19(8), pp. 1386-1396.
- [14] Aghaamoo, M., Aghilinejad, A., Chen, X., 2017, "Numerical study of insulator-based dielectrophoresis method for circulating tumor cell separation", Proc. SPIE 10061, Microfluidics, BioMEMS, and Medical Microsystems XV, 100611A
- [15] Irimajiri, A., Hanai, T., and Inouye, A., 1979, "A dielectric theory of "multi-stratified shell" model with its application to a lymphoma cell", Journal of Theoretical Biology, 78(2), pp. 251-269.